

# UC Berkeley

## UC Berkeley Previously Published Works

### Title

Characterization of Chemisorbed Species and Active Adsorption Sites in Mg–Al Mixed Metal Oxides for High-Temperature CO<sub>2</sub> Capture

### Permalink

<https://escholarship.org/uc/item/46s8m14k>

### Journal

Chemistry of Materials, 34(9)

### ISSN

0897-4756

### Authors

Lund, Alicia  
Manohara, GV  
Song, Ah-Young  
[et al.](#)

### Publication Date

2022-05-10

### DOI

10.1021/acs.chemmater.1c03101

Peer reviewed

# Characterization of Chemisorbed Species and Active Adsorption Sites in Mg-Al Mixed Metal Oxides for High Temperature CO<sub>2</sub> Capture

*Alicia Lund<sup>1,2</sup>, G. V. Manohara<sup>3</sup>, Ah-Young Song<sup>1,2</sup>, Kevin Maik Jablonka<sup>4</sup>, Christopher P. Ireland<sup>4</sup>, Li Anne Cheah<sup>3</sup>, Berend Smit<sup>4</sup>, Susana Garcia<sup>3</sup>, Jeffrey A. Reimer<sup>1,2\*</sup>*

<sup>1</sup> Materials Science Division, Lawrence Berkeley National Laboratory, Berkeley, CA 94720, USA

<sup>2</sup> Department of Chemical and Biomolecular Engineering, University of California, Berkeley, CA 94720, USA

<sup>3</sup> Research Center for Carbon Solutions (RCCS), School of Engineering and Physical Sciences, Heriot-Watt University, Edinburgh, EH14 4AS, UK

<sup>4</sup> Laboratory of Molecular Simulation (LSMO), Institut des Sciences et Ingénierie Chimiques, École Polytechnique Fédérale de Lausanne (EPFL), Rue de l'Industrie 17, Sion, CH-1951, Switzerland

\*Email: reimer@berkeley.edu

## **Abstract**

Mg-Al mixed metal oxides (MMOs), derived from the decomposition of layered double hydroxides (LDHs), have been purposed as adsorbents for CO<sub>2</sub> capture of industrial plant emissions. To aid in the design and optimization of these materials for CO<sub>2</sub> capture at 200 °C, we have used the combination of solid state nuclear magnetic resonance (ssNMR) and density functional theory (DFT) to characterize the CO<sub>2</sub> gas sorption products and determine the various sorption sites in the Mg-Al MMOs. Comparison of DFT cluster calculations with observed <sup>13</sup>C chemical shifts of chemisorbed products indicates that mono and bi-dentate carbonate are formed at those Mg-O sites with adjacent Al substitution of an Mg atom, while bicarbonate is formed at Mg-OH sites without adjacent Al substitution. Quantitative <sup>13</sup>C NMR shows an increase in the relative amount of strongly basic sites, where the monodentate carbonate product is formed, with increasing Al/Mg mole ratio in the MMOs. This detailed understanding of the various basic Mg-O sites presented in MMOs, and the formation of the carbonate, bidentate carbonate and bicarbonate chemisorbed species yields new insight into the mechanism of CO<sub>2</sub> adsorption at 200 °C which can further aid in the design and capture capacity optimization of the materials.

## **Introduction**

Carbon dioxide capture, utilization, and storage (CCUS) are expected to play a key role in reducing the atmospheric CO<sub>2</sub> and mitigate global warming.<sup>1,2</sup> The capture of CO<sub>2</sub> from industrial emissions is one of several approaches towards this end.<sup>3</sup> Solid sorbents such as zeolites,<sup>4</sup> metal-

organic frameworks (MOFs),<sup>5,6</sup> covalent organic frameworks (COFs),<sup>7</sup> mesoporous carbon,<sup>8</sup> and metal oxides<sup>9</sup> have all shown to be promising materials for CO<sub>2</sub> capture. Among the solid CO<sub>2</sub> sorbents, layered double hydroxides (LDHs)-derived mixed metal oxides (MMOs) have shown promising CO<sub>2</sub> capture performance at the 200-500 °C temperature range associated with industrial emissions such as iron and steel plants.<sup>10-13</sup> LDHs derive their structure from the mineral brucite Mg(OH)<sub>2</sub> where partial isomorphous substitution of Mg<sup>2+</sup> ions with higher valent cations (Al<sup>3+</sup>, Fe<sup>3+</sup>, Ga<sup>3+</sup>, etc.) leads to the positively-charged hydroxide layers. Charge-compensating anions, as well as water molecules, are incorporated in the interlayer galleries leading to the formation of the LDHs. LDHs are represented by the general formula [M<sup>2+</sup><sub>1-x</sub>M<sup>3+</sup><sub>x</sub>(OH)<sub>2</sub>]<sup>x+</sup>(A<sup>-x/n</sup>)<sub>n</sub>·yH<sub>2</sub>O, where M<sup>2+</sup>= Mg, Co, Ni, Ca, Zn, M<sup>3+</sup>= Al, Fe, Ga, A= anion (organic or inorganic ions), 0.15 ≤ x ≤ 0.33 and 0.5 ≤ y ≤ 1.0.<sup>14</sup> Due to their physicochemical properties, LDHs and LDH-derived MMOs have proved to be useful materials in various industrial applications including catalysis and sorption.<sup>15-17</sup> The substitution of Mg<sup>2+</sup> with Al<sup>3+</sup> also helps to prevent sintering of the MgO. In the recent past, LDH-derived MMOs have gained prominence as CO<sub>2</sub> capture sorbents due to their high theoretical capture capacity, tolerance to moisture and hydrogen sulfide (H<sub>2</sub>S), ease of preparation/handling, economical cost, and their environmentally friendly nature.<sup>18-22</sup> Interestingly, LDH-derived MMOs have shown unique CO<sub>2</sub> capture performance under both pre- and post-combustion conditions.<sup>23</sup> While the CO<sub>2</sub> capture properties are very promising, the performance of LDH-derived MMOs has yet to live up to the theoretical promise, with measured CO<sub>2</sub> capture capacities are typical in the range of 0.05-1.39 mmol/g.<sup>21</sup> MMOs also have shown poor carbonation/regeneration cycling stability with capture capacities decreasing by 30-50% over 10-20 cycles; overcoming these challenges has been the focus of much ongoing research.<sup>21,24,25</sup>

It is clear from this literature that a detailed atomistic understanding of the CO<sub>2</sub> capture process, including identification of the chemisorbed products, is needed to further drive the development of MMOs for increased capture capacity. Solid-state nuclear magnetic resonance (ssNMR) spectroscopy, and in particular the chemical resolution of magic-angle spinning (MAS), has proven to be a powerful and well established technique for discerning detailed molecular structure and elucidating the host-guest interactions in solid sorbent materials.<sup>26-29</sup> For example, combining multinuclear ssNMR and density functional theory (DFT) chemical shift calculations have been shown to give detailed CO<sub>2</sub> chemisorbed mechanisms in MOFs and porous solid sorbent materials.<sup>30-32</sup> Indeed, extensive NMR studies have been performed on the precursor LDH materials<sup>33</sup> in order to gain structural information such as cation and anion ordering. Yet few studies have focused on the actual MMOs, likely due to their amorphous nature and thus correspondingly broadened NMR linewidths vis-à-vis those in crystalline LDH parent materials. Exploiting multinuclear NMR techniques allows us to take advantage of the distance-dependent dipolar coupling between NMR active guest nuclei and nuclei in the host material; these data, combined with DFT calculations of isotropic chemical shifts, afford insights into the local bonding configurations of MMOs and their interaction with sorbed CO<sub>2</sub>. In this work, we seek to establish the chemisorbed products formed as a result of the interaction between CO<sub>2</sub> and Mg-Al MMOs, and the effect of varying Al content on the chemisorbed products using an *ex situ* <sup>13</sup>CO<sub>2</sub> dosing approach<sup>30</sup>. A detailed adsorption mechanism including whether the chemisorbed products are formed at the Mg or Al sites in the MMOs is also presented.

## Materials and Methods

### *Synthesis and Characterization*

All the reagents,  $\text{Mg}(\text{NO}_3)_2 \cdot 6\text{H}_2\text{O}$ ,  $\text{Al}(\text{NO}_3)_3 \cdot 9\text{H}_2\text{O}$ ,  $\text{Na}_2\text{CO}_3$ ,  $\text{NaOH}$  and nitric acid were purchased from Sigma Aldrich and used as received. Deionized water (18  $\text{M}\Omega$  cm resistivity, Millipore water purification system) was used for all syntheses. Mg-Al- $\text{CO}_3$  LDH with Al/Mg= 0.33, 0.25, 0.20, 0.15) was synthesized by employing the co-precipitation method to yield LDH materials with the formula  $[\text{Mg}_x\text{Al}_{1-x}(\text{OH})_2] (\text{CO}_3)_{x/2} \cdot y\text{H}_2\text{O}$ , S.I. Table 1 reports the actual synthesized formula of each LDH material determined from elemental analysis. In a typical experiment, 3 g of LDH was prepared by slow addition of an aqueous solution of  $\text{Mg}(\text{NO}_3)_2 \cdot 6\text{H}_2\text{O}$  and  $\text{Al}(\text{NO}_3)_3 \cdot 9\text{H}_2\text{O}$  into 500 mL aqueous solution of  $\text{Na}_2\text{CO}_3$  (3 times excess the stoichiometric amount of carbonate). The reaction medium was maintained at pH 10 by adding 1N  $\text{NaOH}$  solution with the help of a Metrohm auto-titrator, 907 Titrando. The reaction mixture was stirred continuously using a magnetic stirrer with the temperature maintained at 70 °C. Once the addition of metal nitrates was complete, the resultant reaction mixture was aged in the mother liquor overnight. The resultant LDH was recovered by centrifugation followed by washing with 1500 mL of water. The product was dried overnight at 70 °C in an oven. The  $\text{CO}_2$  capture studies were performed using a thermogravimetric analyzer (TA Instruments, Discovery series TGA 5500). For  $\text{CO}_2$  capture studies, pristine LDHs were used instead of decomposed ones to avoid  $\text{CO}_2$  contamination. Freshly prepared LDHs were loaded into a TGA pan and decomposed under inert atmosphere (using 100 mL/min  $\text{N}_2$ , 4 h, 400 °C, 10 °C/min). Once the decomposition was completed, the temperature was brought back to 200 °C (10 °C/min) and the gas atmosphere was switched to  $\text{CO}_2$  (for 2 h) to test the uptake capacity of the resultant MMOs under a 90 %  $\text{CO}_2$  atmosphere. For comparison, the  $\text{CO}_2$  capture capacity of  $\text{MgO}$  derived from  $\text{Mg}(\text{OH})_2$  was carried

out identical to the MMOs. To avoid the experimental errors while calculating the CO<sub>2</sub> capture capacities, a blank experiment was conducted by loading an empty pan and the obtained mass gain was subtracted with the actual mass gain for all the MMOs. The MMOs were synthesized by decomposing the LDHs at 400 °C using a muffle furnace (ramp rate = 10 °C/min, residence time = 4 h) under N<sub>2</sub>. Mg(OH)<sub>2</sub> was also calcined under the same conditions to form MgO as a metal oxide reference. After decomposing/calcination the materials were stored in a glove box kept under Ar atmosphere. Complete characterization including ICP-MS, XRD, FTIR, and BET surface area determination of the LDHs and derived MMOs is provided in the supporting information (SI).

**Table 1.** Elemental composition of the LDHs obtained by co-precipitation technique (ICP analysis).

Expected Al/Mg ratio	Experimental Al/Mg ratio	Approximate composition
0.33	0.31	[Mg <sub>0.69</sub> Al <sub>0.31</sub> (OH) <sub>2</sub> ] (CO <sub>3</sub> ) <sub>0.155</sub> · 0.53H <sub>2</sub> O
0.25	0.23	[Mg <sub>0.77</sub> Al <sub>0.23</sub> (OH) <sub>2</sub> ] (CO <sub>3</sub> ) <sub>0.115</sub> · 0.65H <sub>2</sub> O
0.20	0.18	[Mg <sub>0.82</sub> Al <sub>0.18</sub> (OH) <sub>2</sub> ] (CO <sub>3</sub> ) <sub>0.09</sub> · 0.73H <sub>2</sub> O
0.15	0.18	[Mg <sub>0.82</sub> Al <sub>0.18</sub> (OH) <sub>2</sub> ] (CO <sub>3</sub> ) <sub>0.09</sub> · 0.73H <sub>2</sub> O

### *NMR Characterization*

Prior to CO<sub>2</sub> gas dosing, the samples were packed inside the glove box in a 4 mm or 3.2 mm zirconia rotor, then the uncapped rotor was placed into a specialized ex-situ gas dosing system<sup>30</sup> fitted with a tube furnace that allows for <sup>13</sup>CO<sub>2</sub> dosing at 200 °C. Care was taken to ensure the calcined samples were not exposed to air, thus preventing the adsorption of atmospheric water

and/or CO<sub>2</sub>. The uncapped rotors were evacuated for 30 min prior to gas dosing. While held at a constant temperature of 200 °C, the samples were dosed with 1 bar of <sup>13</sup>CO<sub>2</sub> gas (Sigma-Aldrich Carbon-<sup>13</sup>C dioxide < 3 atom % <sup>18</sup>O, 99.0 atom % <sup>13</sup>C) and allowed to equilibrate for 1 hr. The rotor was then cooled to 120 °C and the Kel-F cap was quickly placed on the rotor without exposing the dosed material to atmosphere, and the sealed 4 mm rotor was inserted into a 11.74 T magnet (500 MHz <sup>1</sup>H Larmor frequency, Avance I Bruker spectrometer) with a Bruker dual channel CPMAS probe and. The TRAPDOR measurements were performed in a 16.4 T (700 MHz <sup>1</sup>H Larmor frequency, Bruker Avance I spectrometer) with a 3.2 mm Bruker triple channel <sup>1</sup>H/<sup>13</sup>C/<sup>15</sup>N probe. All NMR measurements were performed at room temperature with a MAS rate of 10 kHz. All spectral deconvolution, including quadrupolar and chemical shift parameters, were determined using the spectral fitting software Dmfit.<sup>34</sup>

A rotor synchronized DEPTH<sup>35</sup> pulse sequence was employed to remove the background <sup>1</sup>H signal and quantitate the <sup>1</sup>H spectrum, with a radio field (*rf*) strength of 57 kHz, and a recycle delay of 2s, equivalent to 5T<sub>1</sub>. Quantitative <sup>13</sup>C measurements were performed using a single pulse with *rf* strength of 75 kHz and proton decoupling (50 kHz strength) during acquisition with a recycle delay of 600s, equivalent to 5T<sub>1</sub>. The 1D <sup>1</sup>H-<sup>13</sup>C cross polarization (CP) spectra were measured with a contact time of 2 ms and a *rf* strength of 70 kHz <sup>1</sup>H and a ramp 30 to 50 kHz <sup>13</sup>C *rf* field strength and a <sup>1</sup>H decoupling power of 80 kHz during detection. The 2D <sup>1</sup>H-<sup>13</sup>C heteronuclear correlation spectra were measured with a contact pulse of 200 μs to probe only the <sup>1</sup>H in spatial proximity to the chemisorbed <sup>13</sup>CO<sub>2</sub> species. Frequency switched Lee-Goldberg decoupling was applied during the <sup>1</sup>H evolution period at 80 kHz *rf* strength.<sup>36</sup> Multiple quantum magic-angle spinning (MQMAS) <sup>27</sup>Al NMR measurements were also performed on the MMOs before and after



gas dosing. An *rf* strength of 180 kHz for the  $^{27}\text{Al}$  measurements was used, the quantitative single pulse measurements using a small flip angle of 30 degrees to insure NMR signal intensity was not affected by differences in quadrupolar coupling frequencies of the  $^{27}\text{Al}$  environments. The *z*-filtered MQMAS sequence was used with a selective 90 pulse of 30 kHz *rf* strength.<sup>37</sup> Adamantane was used as an external reference for both the  $^1\text{H}$  and  $^{13}\text{C}$  chemical shifts and 0.1 M  $\text{Al}(\text{NO}_3)_3(\text{aq})$  was used for the chemical shift and *rf* strength calibration of  $^{27}\text{Al}$ . The TRAPDOR measurements were performed at a magnetic field strength of 16.4 T. Here the standard Hahn-echo sequence ( $90-\tau-180-\tau$ ) was used to collect the rotor synchronized  $^1\text{H}$  echo and during the first  $\tau$  period continuous wave  $^{27}\text{Al}$  irradiation was applied at a *rf* strength of 160 kHz. Each subsequent step  $\tau$  was incremented by a multiple of the rotor period and the  $^1\text{H}$  Hahn echo was recorded with and without  $^{27}\text{Al}$  irradiation.

### *DFT Simulation Parameters*

Density Functional Theory (DFT) calculations of isotropic chemical shifts were conducted to get insights into the local bonding configurations of MMOs and their interaction with sorbed  $\text{CO}_2$ . The starting structure for the simulation of the MMO cluster was a cubic  $\text{MgO}$  cluster as described in literature.<sup>38</sup> The B3LYP hybrid functional with the double-valence double-zeta polarized basis set 6-31++G\*\* was chosen as the hybrid functional and basis set as it has been shown to be suitable for qualitative trends in MMO cluster calculations.<sup>39,40</sup> Simulations were orchestrated using the AiiDA workflow manager<sup>41</sup> and the DFT calculations were performed using Gaussian 16;<sup>42</sup> for convergence the YQC algorithm was used. NMR shifts were calculated using the gauge independent atomic orbital (GIAO) formalism.<sup>43</sup> The dimer trimethylaluminum was used as a

reference for determining the chemical shift from the chemical shielding calculations. Chemical shifts are reported at  $\delta_{iso} = \sigma_{ref} - \sigma_{iso}$ .

## Results and Discussion

### *Chemisorption Mechanism*

The direct  $^{13}\text{C}$  NMR spectra of the  $^{13}\text{CO}_2$  - dosed MMOs and MgO (Figure 1) presents two distinct regions of observed  $^{13}\text{C}$  chemical shifts. The peak at 125.1 ppm is assigned to physisorbed  $\text{CO}_2$  as it agrees well with previously reported chemical shifts of physisorbed  $\text{CO}_2$  in similar LDH and crystalline MgO materials.<sup>44,45</sup> The peaks in the region 160-170 ppm are assigned to chemisorbed carbonate and bicarbonate species by comparison to known shifts of such compounds.<sup>46-48</sup>

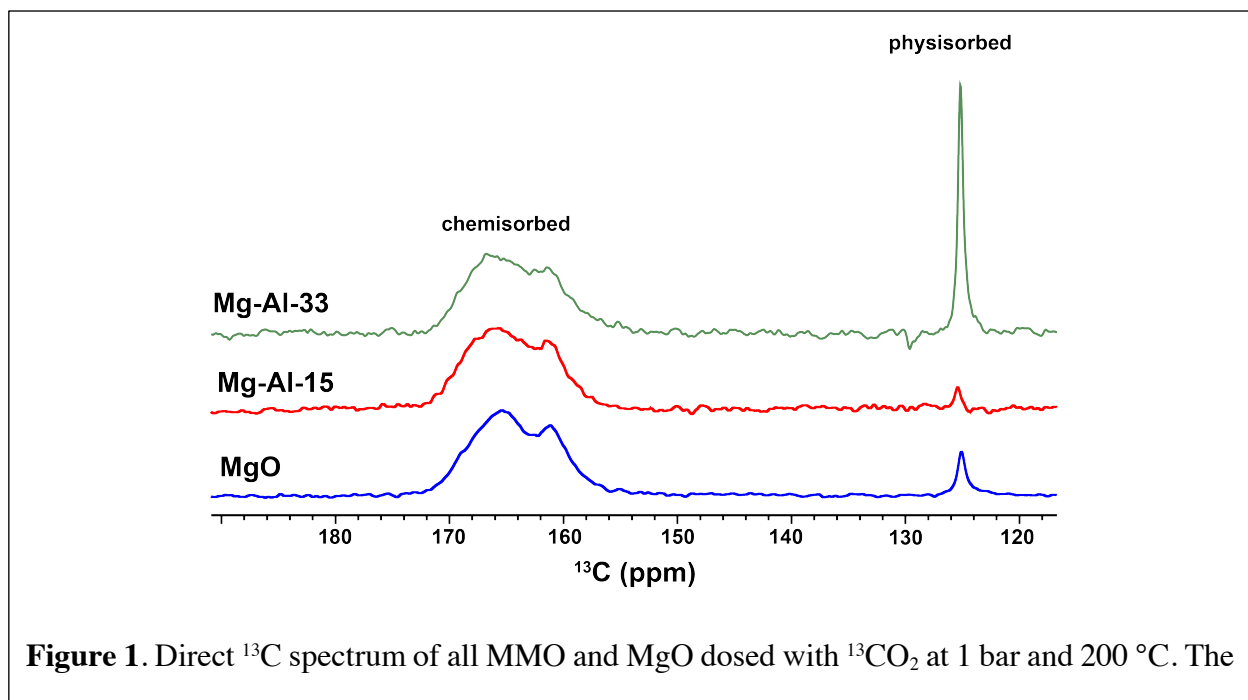
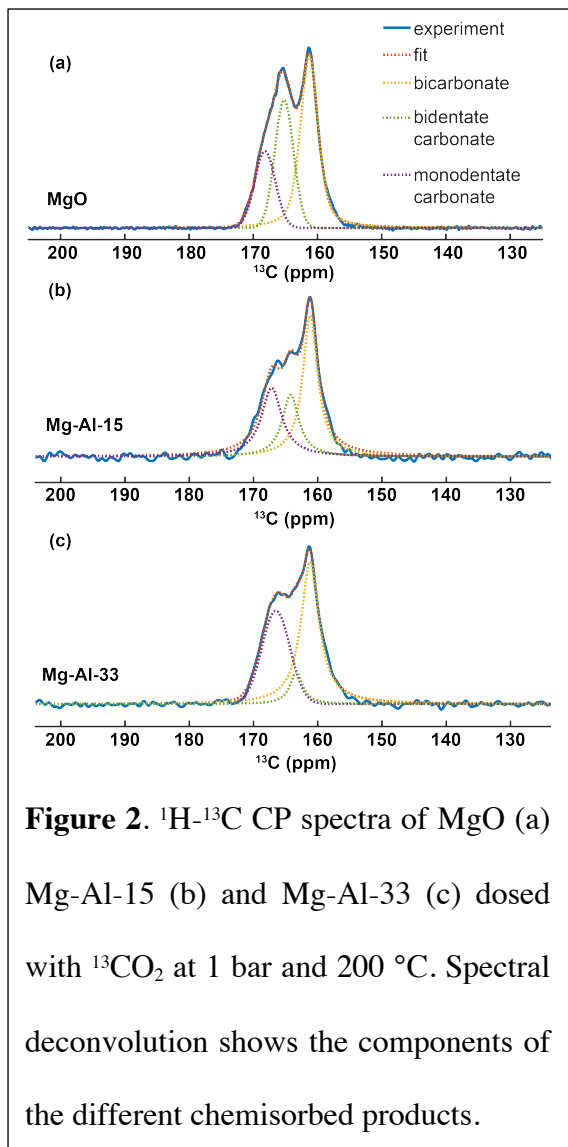


**Figure 1.** Direct  $^{13}\text{C}$  spectrum of all MMO and MgO dosed with  $^{13}\text{CO}_2$  at 1 bar and 200 °C. The



Analysis of the integral in the quantitative  $^{13}\text{C}$  NMR spectra shows the chemisorbed  $\text{CO}_2$  comprises between 80-93% of the  $\text{CO}_2$  adsorbed in the MMOs. The  $^1\text{H}$ - $^{13}\text{C}$  CP spectra for  $^{13}\text{CO}_2$  dosed MMOs with Al content of Al/Mg = 0.15 and 0.33 denoted Mg-Al-15 and Mg-Al-33 respectively, and decomposed MgO are shown in Figure 2. The CPMAS spectrum measures the  $^{13}\text{C}$  signal of those species that are strongly dipolar coupled to  $^1\text{H}$  spins in the MMOs framework and reveals only the chemisorbed species since the physisorbed  $\text{CO}_2$  exhibits negligible  $^1\text{H}$  dipolar coupling. In the 1D  $^{13}\text{C}$  CPMAS spectra of all the dosed materials three chemisorbed species can be identified through a spectral decomposition. The first peak is observed at 161 ppm for both Mg-Al-15 and Mg-Al-33, and

2D  $^1\text{H}$ - $^{13}\text{C}$  HETCOR spectra (Figure 3) show a strong correlation of this peak to the bicarbonate proton at  $^1\text{H}$  (~5.5 ppm). The bicarbonate  $^{13}\text{C}$  and  $^1\text{H}$  chemical shifts observed herein match the literature values of bicarbonate species in other MgO crystalline structures.<sup>46,48</sup> To confirm that this bicarbonate species were formed via chemisorption of  $\text{CO}_2$  and not a residual product formed from incomplete decomposition of the LDH starting material, S.I.1 shows the  $^1\text{H}$  quantitative NMR spectra before and after  $^{13}\text{CO}_2$  adsorption. The clear formation of bicarbonate proton can be seen after the  $\text{CO}_2$  adsorption at 5.5 ppm. IR measurements performed before and after calcination of

the LDH material, (S.I. 2 & 5) also confirmed the complete removal of the carbonate anion from the LDH upon calcination.

The other two spectroscopically resolved  $^{13}\text{C}$  species are carbonate/MMOs species appearing at  $^{13}\text{C}$  chemical shifts of 167.2 and 165.1 ppm in Mg-Al-15, and 166.5 and 163.3 ppm for Mg-Al-33. We assigned the higher ppm shifted carbonate species (167.2, 166.5 ppm) to monodentate carbonate and lower shifted carbonate peaks (165.1, 163.3 ppm) to bidentate carbonate based upon previous IR and NMR characterization<sup>9,48</sup> of heat-treated MgO where the presence of multiple carbonate species formed upon  $\text{CO}_2$  dosing at elevated temperatures were assigned to both mono- and bidentate carbonate species. In those studies, the reported  $^{13}\text{C}$  chemical shift for mono- and bidentate carbonate in MgO are 168 and 164 ppm, respectively, and agree well those reported herein.

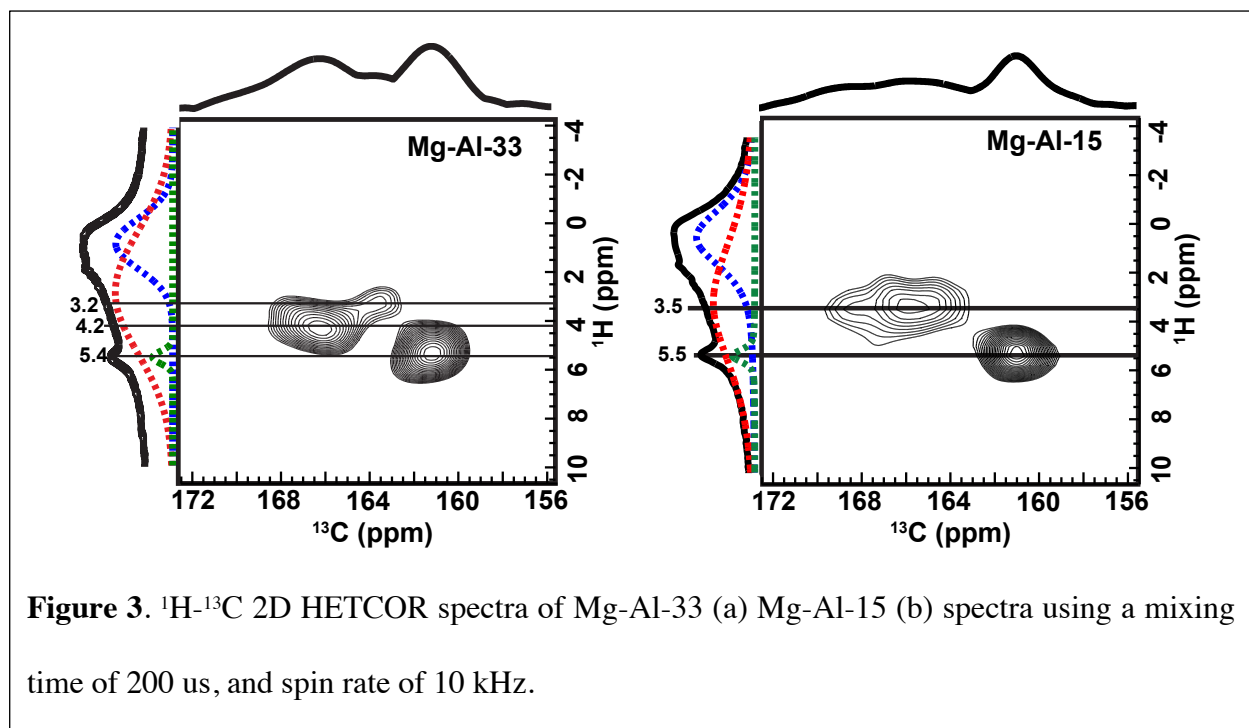


**Figure 3.**  $^1\text{H}$ - $^{13}\text{C}$  2D HETCOR spectra of Mg-Al-33 (a) Mg-Al-15 (b) spectra using a mixing time of 200 us, and spin rate of 10 kHz.

The 2D HETCOR spectra for Mg-Al-15 shows both carbonate peaks correlate with a  $^1\text{H}$  NMR peak centered at  $\sim 3.5$  ppm; this agrees well with the peak at 3.4 ppm in the  $^1\text{H}$  quantitative spectra (as seen in the projection of the  $^1\text{H}$  dimension in Figure 3). We attribute this broad correlation of the two carbonate species to the protons of mixed metal hydroxide  $\text{MgAlOH}$ . Studies of hydroxyl groups in Mg-Al LDHs with varying Al/Mg ratio from 0.19-0.33 showed the  $^1\text{H}$  hydroxide group associated with the Al-Mg cluster ranged between 2.9 – 4 ppm,<sup>49</sup> in good agreement with the broad proton resonance observed in the 2D HETCOR of the MMOs presented here and quantitative  $^1\text{H}$  spectra centered at 3.5 ppm.

The Mg-Al-33 carbonate species are correlated with broad proton resonances at 3.2 and 4.2 ppm; the latter increased proton shift is associated with the increased acidity of the mixed metal hydroxide group with increasing amounts of  $^{27}\text{Al}$  in the material, as has been observed in the parent LDH material.<sup>50</sup> An additional peak is observed in the  $^1\text{H}$  quantitative spectra for both Mg-Al-15 and Mg-Al-33 that is attributed to the hydroxyl group associated with the  $\text{MgOH}$  observed at a range of 0.9-0 ppm.<sup>49-51</sup> No correlation of the carbonated species was observed with these  $\text{MgOH}$  hydroxyl groups in the dosed MMOs. Thus, a combination of 1D and 2D  $^1\text{H}$ - $^{13}\text{C}$  NMR study of MMOs dosed with  $\text{CO}_2$  at elevated temperatures leads us to the conclusion that there exist multiple chemisorbed products in the material; monodentate and bidentate carbonate, and bicarbonate. The 2D HETCOR spectrum of MMOs shows both mono- and bidentate carbonate species are correlated to the mixed metal hydroxide,  $\text{MgAlOH}$ , likely due to an electrostatic interaction between the Al substitution site and the carbonate. The HETCOR establishes a proximity between the mono- and bidentate carbonate species and the Al substitution site. The exact role of the  $\text{MgAlOH}$  protons in the material on the carbonate formation are beyond the scope of this study.

### Quantum chemical mechanistic implications

We turn to quantum chemical calculations to further assess the formation of the carbonate and bicarbonate in the mixed metal oxides. Literature studies have proposed multiple CO<sub>2</sub> adsorption sites in the LDHs and the derived MMOs materials.<sup>9,44,49</sup> From these studies multiple mechanisms have been proposed for the formation of the CO<sub>2</sub> adsorption sites, such as the decomposition of the active Mg-O species wherein Al<sup>3+</sup> substitutes for Mg<sup>2+</sup> in the MgO lattice leading to a coordinately unsaturated adjacent oxygen atom that in turn becomes the basic sites for CO<sub>2</sub> chemisorption. Another proposed mechanism proposes diffusion of Al out of the octahedral MgO layers leaving a vacancy site where the Mg-O active species is formed. We test these hypotheses by considering DFT calculated <sup>13</sup>C chemical shifts of the chemisorbed CO<sub>2</sub> species adjacent to an Al<sup>3+</sup> substitution site in the MMOs. Creating a reliable DFT model can

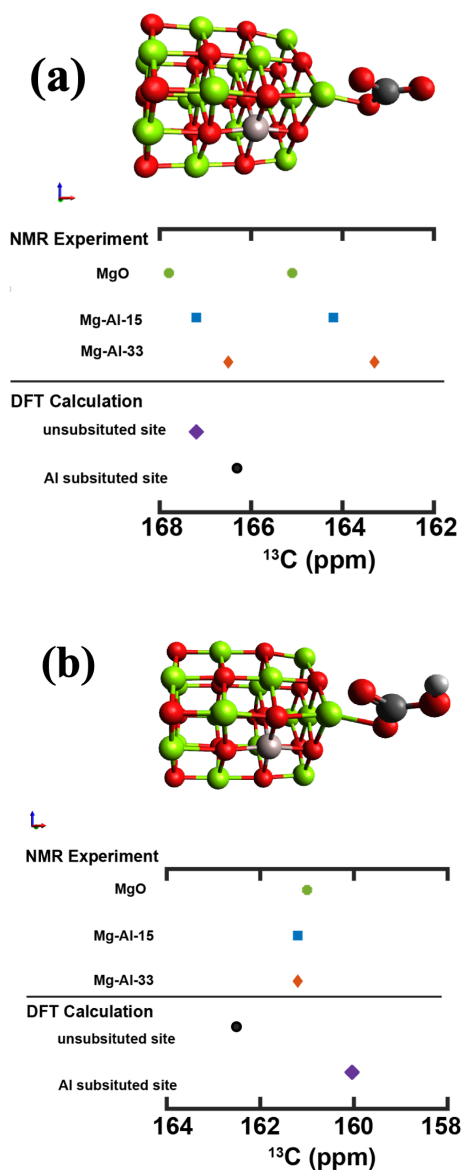


**Figure 4.** Comparison of experimentally measured and DFT calculated <sup>13</sup>C chemical shifts for the cubic MgO structure with and without adjacent Al substitution for carbonate (a) and bicarbonate (b). Mg (green), O (red), Al (light brown), C (dark grey), H (light grey).

be difficult, however, due to the complex atomic structure of the MMOs. Here we take the approach used previously<sup>52,39</sup> where cluster models are imagined to examine specific sites in the MMOs material. The model system used for the simulations is based upon the cubic MgO structure.<sup>38</sup> Thus these simulations are not to propose an exact structure for the MMO system, but rather to mimic the effect of site-specific substitution of Mg<sup>2+</sup> with Al<sup>3+</sup> on the <sup>13</sup>C chemical shifts of the chemisorbed species. Here we seek to discern which chemisorbed species are adjacent to an Al sites by taking a corner Mg site in a MgO cubic cluster and substituting it with an Al atom as shown in Figure 4 (a,b). The <sup>13</sup>C chemical shift of either carbonate and bicarbonate species at the Mg corner site was then calculated with and without this Al substitution.

A comparison of the DFT and experimental NMR <sup>13</sup>C chemical shifts of the *carbonate* species is shown in Figure 4(a). The experimental <sup>13</sup>C NMR isotropic chemical shift of the carbonate species decreases 1-2 ppm with increasing Al content: from 168 ppm in the decomposed MgO to 167.7 ppm in Mg-Al-15, to 166.5 ppm in Mg-Al-33 for the monodentate carbonate species; from 165.1 ppm to 163.3 ppm for the bidentate carbonate species. The experimentally observed change in isotropic shifts of 2 ppm with increasing Al content agrees well with DFT-calculated shifts of 167.2 ppm in the unsubstituted MgO cluster and 166.5 ppm with the Al substitution. This change in <sup>13</sup>C isotropic chemical shift with the Al substitution further demonstrates that both the mono- and bidentate carbonate species are more favorably formed at a Mg-O site with an adjacent Al substitution, as opposed to isolated Mg-O sites.

For the *bicarbonate* species the same analysis was performed, shown in Figure 4(b), where DFT calculations of the <sup>13</sup>C isotropic chemical shift of bicarbonate in Mg-O are shown with and without

an adjacent Al substitution. In contrast to the carbonate signal, increasing Al content does not show a significant change in the experimentally determined bicarbonate chemical shift (~ 161 ppm for all experimentally measured shifts). The DFT calculated chemical shifts for the unsubstituted and Al substituted bicarbonate species, however, shows a shift from 160.0 to 162.5 ppm, respectively. The unchanged experimentally determined bicarbonate  $^{13}\text{C}$  chemical shift, regardless of Al content in the material, further supports our hypothesis that the bicarbonate species are formed from basic  $\text{Mg}_3\text{OH}$  sites and are not dependent on the Al substitution.

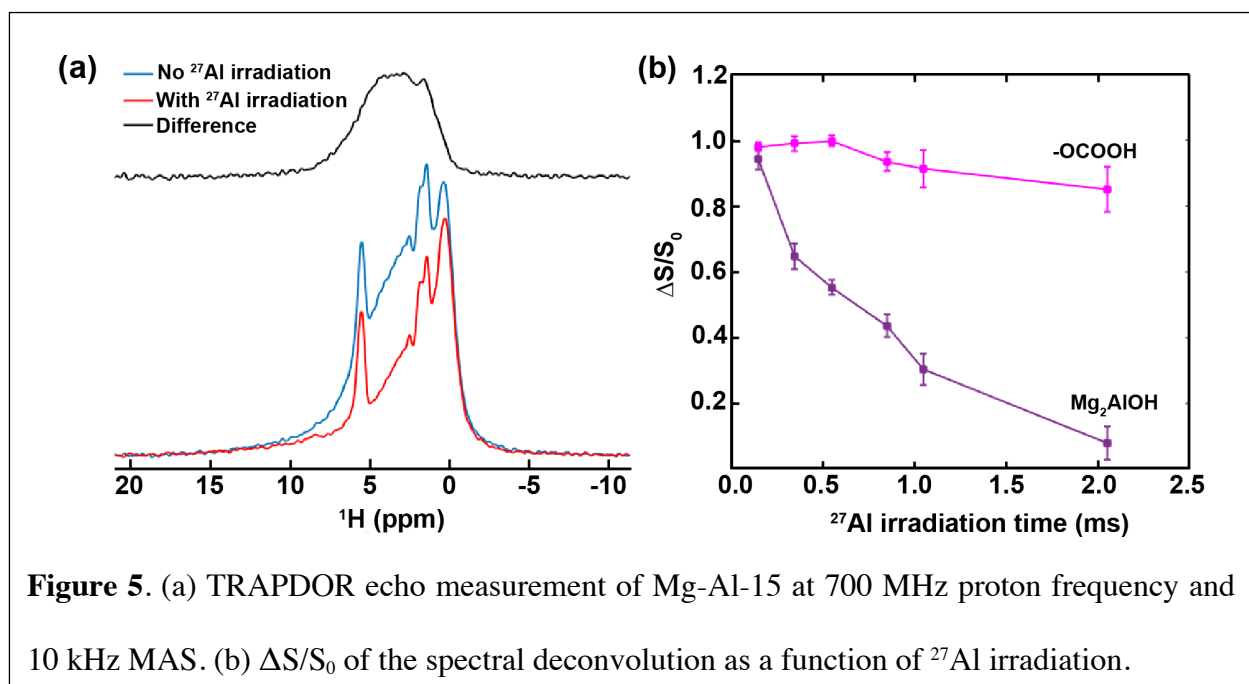
**Table 2.** DFT calculated  $^{13}\text{C}$  chemical shifts (in ppm) for cubic  $\text{Mg}_{14}\text{Al}_4\text{O}_{18}$ ,  $\text{Mg}_{17}\text{AlO}_{18}$ , and  $\text{MgO}$ .

	Cubic $\text{Mg}_{14}\text{Al}_4\text{O}_{18}$	Cubic MgO w/Al substitution $\text{Mg}_{17}\text{AlO}_{18}$	Cubic MgO $\text{Mg}_{18}\text{O}_{18}$
bicarbonate	160.5	162.5	160.0
carbonate	168.8	166.3	167.2

While the model system does estimate the effect of a single site Al substitution on carbon chemical shifts, this cluster is not representative of the actual Mg/Al ratios the MMO systems use here. We addressed this by randomly sampling carbonate and bicarbonate locations at 50 different Al positions in the cubical  $\text{Mg}_{14}\text{Al}_4\text{O}_{18}$  system. The geometry was optimized and the resulting lowest energy configuration was used for the chemical shift calculation (Table 2). In structures with higher Al content the carbonate species were located at oxygen atoms between two Mg with a large distortion in the cubic structure of the MMO. The large distortion in the cubic metal oxide structure with increasing Al content likely leads to the difference in chemical shift between the DFT  $^{13}\text{C}$  chemical shift calculations and those determined experimentally.



This hypothesis is further supported by consideration of the spatial proximity of Al to the bicarbonate moiety via  $^1\text{H}$ - $^{27}\text{Al}$  TRAPDOR, a methodology whereby rotationally-refocused echoes of the  $^1\text{H}$  spins during the MAS rotor period are interlaced with  $^{27}\text{Al}$  excitation. During the first evolution period continuous wave irradiation is applied to the  $^{27}\text{Al}$  spins leading to a reintroduction of the dipolar interaction between proximate  $^1\text{H}$ - $^{27}\text{Al}$  pairs, causing a dephasing or reduced intensity of the  $^1\text{H}$  species coupled the  $^{27}\text{Al}$  spin.<sup>50,53</sup> Figure 5 shows the refocused  $^1\text{H}$  echoes with and without  $^{27}\text{Al}$  irradiation and the difference between the two spectra. Here normalization of the refocused echoes with and without irradiation considers signal reduction due to  $T_2$ , and error bars for each irradiation period were calculated from the signal-to-noise ratio of each echo spectrum. The difference spectra show a broad peak centered at 3.1 ppm attributed to the mixed metal



hydroxyl groups, establishing the spatial correlation of these protons with aluminum ions. Importantly, the bicarbonate proton at 5.5 ppm is not affected by  $^{27}\text{Al}$  irradiation. Figure 5(b) shows a plot of the  $\Delta S/S_0$  of the bicarbonate  $^1\text{H}$  and mixed metal hydroxide showing that the bicarbonate

proton remains largely undisturbed by  $^{27}\text{Al}$  irradiation. DFT simulations of bicarbonate species formed at MgO sites with an adjacent Al yield an approximate  $^1\text{H}$ - $^{27}\text{Al}$  distance of 6.8 Å, revealing that if the bicarbonate is formed at a  $\text{Mg}_2\text{AlOH}$  site the bicarbonate peak should exhibit a TRAPDOR dephasing effect. From the combination of  $^{13}\text{C}$  chemical shift calculations for Mg-O carbonate with and without an adjacent Al site, in combination with the heteronuclear correlation data from TRAPDOR, we conclude that both the mono- and bidentate carbonate species preferentially form at Mg-O sites with adjacent Al substitution. In contrast, the bicarbonate species are preferentially formed at Mg-OH sites in the material without Al substitution, likely at basic  $\text{Mg}_3\text{OH}$  sites in the MMO material.

#### *The role of Al content on the $\text{CO}_2$ capture capacity*

The  $\text{CO}_2$  capture capacities of the MMOs were tested via gravimetric methods as detailed in the experimental section above and are given in the Figure 6. The observed capture capacities were in the range of 0.45 to 0.82 mmol/g, where the 0.25 Al/Mg sample shows the highest  $\text{CO}_2$  capture capacity of 0.82 mmol/g. These observations are in line with the literature reported values for the LDH derived MMOs.<sup>54,55</sup> For comparison we also report the  $\text{Mg}(\text{OH})_2$  derived MgO  $\text{CO}_2$  capture capacity of 1.36 mmol/g. While the initial capture capacity of the MgO is larger than the Al-Mg MMOs, it has been reported in the literature that the capture capacity drops off rapidly with increasing number of cycles in the MgO material when compared with Al-Mg MMOs.<sup>56</sup>

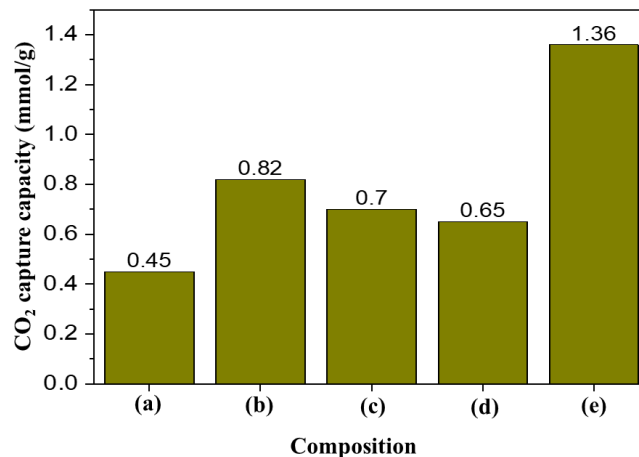
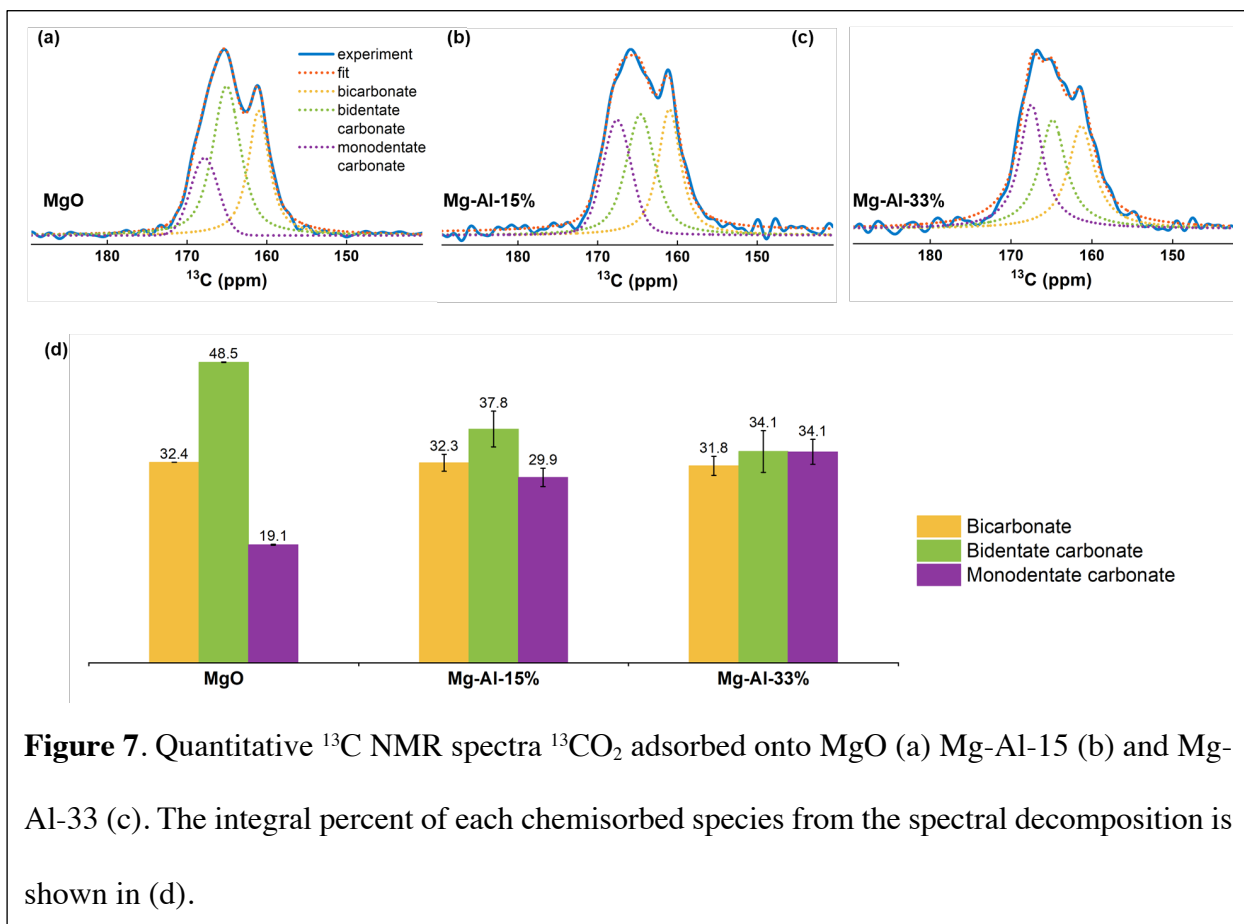


**Figure 6.** CO<sub>2</sub> capture capacity (200 °C, 2h, 90 % CO<sub>2</sub>) of MMOs generated from Mg-Al-CO<sub>3</sub> LDHs prepared by co-precipitation at pH 10 with varied Al/Mg (a) 0.33, (b) 0.25, (c) 0.20, (d) 0.15. (e) is Mg(OH)<sub>2</sub>

To further address the role of Al we quantitate the distribution of chemisorbed products formed after high temperature CO<sub>2</sub> adsorption. We therefore analyzed the direct quantitative <sup>13</sup>C NMR spectra of CO<sub>2</sub> sorbed onto decomposed MgO, Mg-Al-15 and Mg-Al-33. These quantitative <sup>13</sup>C spectra were fit using Dmfit software with a mixture of Gaussian and Lorentzian line shapes, and the results of the spectra decompositions are summarized in Figure 7. The different carbonate and bicarbonate species form at a diverse range of basic sites in the MgO material with the bicarbonate formed at weakly basic MgOH sites, bidentate carbonate formed at medium basic sites, and strongly basic sites forming monodentate carbonate.<sup>48</sup> The dominant chemisorbed product formed with <sup>13</sup>CO<sub>2</sub> dosing at 200 °C onto MgO is bidentate carbonate (49% of the NMR signal intensity), 19% for the monodentate carbonate, and 32% associated with bicarbonate formation. This agrees with previous work showing moderately basic sites are the predominant CO<sub>2</sub> adsorption sites in MgO, which forms the bidentate carbonate chemisorbed product.<sup>48</sup>



The Mg-Al-15 MMO structure exhibits a 38% reduction in the bidentate carbonate component, while the monodentate carbonate signal increased to make up 28%, with the bicarbonate species making up 34% of the chemisorbed product in the  $^{13}\text{C}$  quantitative spectrum. As the Al content is increased further in the Mg-Al-33 MMOs, the bidentate carbonate is further reduced to 34%, and the monodentate carbonate signal again increases to 34%, while the bicarbonate signal is also reduced to 32% of the total  $^{13}\text{C}$  chemisorbed product. We find a general trend of increasing relative monodentate carbonate signal with increasing Al content in these MMOs, consistent with the hypothesis that Al substitution creates strongly basic sites leading to a more favorable formation association of the monodentate carbonate species with these sites. In addition, this increase in formation of strong basic Mg-O sites with increasing Al content appears to be also associated with

a reduction with moderately basic sites in the material, as evidenced by the decrease in relative amount of bidentate carbonate sites with increasing Al content. The bicarbonate species are formed at the weak basic Mg-OH sites in the material, likely due to the calcination method causing partial dihydroxylation and removal of surface bound water, and thus shows only slight variation in relative amount with Al content. With this context, we can examine the trend shown in figure 6 where increasing Al from 0.15 to 0.25 mole shows a general trend in increasing the CO<sub>2</sub> capture capacity. Thus one possibility for increasing capacity would be to increase the relative amount of strongly basic sites in the MMO material. Increasing the Al content further to 0.33 shows a decrease in the CO<sub>2</sub> capture capacity of the MMO even with a further increase in relative amount of strongly basic sites in the MMO. This could be due to a drop in the absolute amount of adsorption sites available in the material; in addition, an increase in the Al content causes a decrease in the surface area of the MMO material, as measured by BET adsorption (S.I. Table 1). Finally, we characterized the Al structure in the material directly through <sup>27</sup>Al MQMAS NMR as detailed in S.I.10&11 The resulting isotropic shifts and quadrupolar parameters agree well with previously reported values in the literature.<sup>49,54,57,58</sup>

## **Conclusion**

Analysis of solid-state <sup>13</sup>C NMR spectra allows identification of mono- and bidentate carbonates and bicarbonates upon CO<sub>2</sub> adsorption onto Mg-Al MMOs. The comparison of DFT cluster calculations with changes in <sup>13</sup>C chemical shift with changing increasing Al/Mg ratio supports the hypothesis that the mono- and bidentate carbonate species are formed at the Mg-Al mixed metal oxide sites, while the bicarbonate is formed at weakly basic Mg-OH sites. These calculations are

confirmed via proton-aluminum double resonance measurements. Quantitative  $^{13}\text{C}$  NMR enumerates the ratios of chemisorbed species with increasing Al/Mg ratio and reveals that the relative amount of monodentate carbonate increases with increasing Al content, confirming the association of Al with strong basic sites in the MMOs. This detailed understanding of the various basic sites present in the MMO material, and the formation of different chemisorbed species, yields new insight into the mechanism of  $\text{CO}_2$  adsorption. With this understanding of the  $\text{CO}_2$  chemisorbed mechanism, as well as further studies on the optimal synthesis and decomposition methods, we anticipate that increasing basic site availability without sacrificing surface area and capacity will afford the full potential of MMOs for  $\text{CO}_2$  capture applications.

## ASSOCIATED CONTENT

### **Supporting Information**

The Supporting Information is available free of charge.

ICP analysis, PXRD, FTIR, TGA of the synthesized Mg/Al LDHs, and PXRD, FTIR,  $\text{N}_2$  adsorption isotherms of the MMOs generated from Mg- $\text{AlCO}_3$  LDHs; Quantitative  $^1\text{H}$  NMR,  $^{27}\text{Al}$  MQMAS before and after  $^{13}\text{CO}_2$  adsorption in MMOs; and the calculated energies of DFT simulations

## AUTHOR INFORMATION

### **Corresponding Author**

**Jeffrey A. Reimer** - Materials Sciences Division, Lawrence Berkeley National Laboratory, Berkeley, California 94720, United States; Department of Chemical and Biomolecular Engineering and College of Chemistry, University of California, Berkeley, California 94720, United States; <https://orcid.org/0000-0002-4191-3725>; Email: [reimer@berkeley.edu](mailto:reimer@berkeley.edu)

### **Authors**

**Alicia Lund** - Materials Science Division, Lawrence Berkeley National Laboratory, Berkeley, CA 94720, United States; Department of Chemical and Biomolecular Engineering, University of California, Berkeley, CA 94720, United States; <https://orcid.org/0000-0001-7520-9544>

**G. V. Manohara** - Research Center for Carbon Solutions (RCCS), School of Engineering and Physical Sciences, Heriot-Watt University, Edinburgh, EH14 4AS, United Kingdom; <https://orcid.org/0000-0003-3817-6610>

**Ah-Young Song** - Materials Science Division, Lawrence Berkeley National Laboratory, Berkeley, CA 94720, United States; Department of Chemical and Biomolecular Engineering, University of California, Berkeley, CA 94720, United States; <https://orcid.org/0000-0001-7931-0148>

**Kevin Maik Jablonka** - Laboratory of Molecular Simulation (LSMO), Institut des Sciences et Ingénierie Chimiques, École Polytechnique Fédérale de Lausanne (EPFL), Rue de l'Industrie 17, Sion, CH-1951, Switzerland; <https://orcid.org/0000-0003-4894-4660>

**Christopher P. Ireland** - Laboratory of Molecular Simulation (LSMO), Institut des Sciences et Ingénierie Chimiques, École Polytechnique Fédérale de Lausanne (EPFL), Rue de l'Industrie 17, Sion, CH-1951, Switzerland; <https://orcid.org/0000-0002-2436-3987>

**Li Anne Cheah** - Research Center for Carbon Solutions (RCCS), School of Engineering and Physical Sciences, Heriot-Watt University, Edinburgh, EH14 4AS, United Kingdom

**Berend Smit** - Laboratory of Molecular Simulation (LSMO), Institut des Sciences et Ingénierie Chimiques, École Polytechnique Fédérale de Lausanne (EPFL), Rue de l'Industrie 17, Sion, CH-1951, Switzerland; <https://orcid.org/0000-0003-4653-8562>

**Susana Garcia** - Research Center for Carbon Solutions (RCCS), School of Engineering and Physical Sciences, Heriot-Watt University, Edinburgh, EH14 4AS, UK; <https://orcid.org/0000-0002-3713-311X>

## **Acknowledgments**

The PrISMa Project (No 299659) is funded through the ACT programme (Accelerating CCS Technologies, Horizon2020 Project No 294766). Financial contributions made from: Department for Business, Energy & Industrial Strategy (BEIS) together with extra funding from NERC and EPSRC research councils, United Kingdom; The Research Council of Norway, (RCN), Norway; Swiss Federal Office of Energy (SFOE), Switzerland; and US-Department of Energy (US-DOE), USA, are gratefully acknowledged. Financial support from TOTAL and Equinor is also gratefully acknowledged. We thank Dr. Hasan Celik and UC Berkeley's NMR facility in the College of Chemistry (CoC-NMR) for spectroscopic assistance.



## References

1. Smit, B.; Reimer, J. A.; Oldenburg, C. M.; Bourg, I. C. *Introduction to Carbon Capture and Sequestration*; Imperial College Press: London, UK, 2014.
2. Smit, B.; Garcia, S. Carbon capture and storage: making fossil fuels great again?. *Europhys. News* **2020**, *51*, 20 - 22.
3. Bui, M.; Adjiman, C. S.; Bardow, A.; Boston, A.; Brown, S.; Fennell, P. S.; Fuss, S.; Galindo, A.; Hackett, L. A.; Hallett, J. P.; Herzog, H. J.; Jackson, G.; Kemper, J.; Krevor, S.; Maitland, G. C.; Matuszewski, M.; Metcalfe, I. S.; Petit, C.; Puxty, G.; Reimer, J.; Reiner, D. M.; Rubin, E. S.; Scott, S. A.; Shah, N.; Smit, B.; Trusler, J.; Webley, P.; Wilcox, J.; Dowell, N. M. Carbon capture and storage (CCS): The way forward. *Energy Environ. Sci.* **2018**, *11*, 1062 - 1176.
4. Murge, P.; Dinda, S.; Roy, S. Zeolite-Based Sorbent for CO<sub>2</sub> Capture: Preparation and Performance Evaluation. *Langmuir* **2019**, *35*, 14751 - 14760.
5. Saha, S.; Chandra, S.; Garai, B.; Banerjee, R. Carbon dioxide capture by metal organic frameworks. *Indian J. Chem.* **2012**, *51*, 1223 - 1230.
6. Trickett, C. A.; Helal, A.; Al-Maythaly, B. A.; Yamani, Z. H.; Cordova, K. E.; Yaghi, O. M. The chemistry of metal-organic frameworks for CO<sub>2</sub> capture, regeneration and conversion. *Nat. Rev. Mater.* **2017**, *2*, 17045.
7. An, S.; Xu, T.; Peng, C.; Hu, J.; Liu, H. Rational design of functionalized covalent organic frameworks and their performance towards CO<sub>2</sub> capture. *RSC Adv.* **2019**, *9*, 21438 - 21443.

8. Wang, J.; Huang, H.; Wang, M.; Yao, L.; Qiao, W.; Long, D.; Ling, L. Direct capture of low-concentration CO<sub>2</sub> on mesoporous carbon-supported solid amine adsorbents at ambient temperature. *Ind. Eng. Chem. Res.* **2015**, *54*, 5319 - 5327.
9. Gao, Y.; Zhang, Z.; Wu, J.; Yi, X.; Zheng, A.; Umar, A.; O'Hare, D.; Wang, Q. Comprehensive investigation of CO<sub>2</sub> adsorption on Mg-Al-CO<sub>3</sub> LDH-derived mixed metal oxides. *J. Mater. Chem. A* **2013**, *1*, 12782 - 12790.
10. Sharma, U.; Tyagi, B.; Jasra, R. V. Synthesis and characterization of Mg-Al-CO<sub>3</sub> layered double hydroxide for CO<sub>2</sub> adsorption. *Ind. Eng. Chem. Res.* **2008**, *47*, 9588 - 9595.
11. Ram Reddy, M. K.; Xu, Z. P.; Lu, G. Q.; Da Costa, J. C. D. Layered double hydroxides for CO<sub>2</sub> capture: Structure evolution and regeneration. *Ind. Eng. Chem. Res.* **2006**, *45*, 7504 - 7509.
12. Flores-Granobles, M.; Saeys, M. Minimizing CO<sub>2</sub> emissions with renewable energy: A comparative study of emerging technologies in the steel industry. *Energy Environ. Sci.* **2020**, *13*, 1923 - 1932.
13. Van Dijk, H. A. J.; Cobden, P. D.; Lukashuk, L.; Water, L. v.; Lundqvist, M.; Manzoloni, G.; Cormos, C.; van Dijk, C.; Mancuso, L.; Johns, J.; Bellqvist, D. Stepwise project: Sorption-enhanced water-gas shift technology to reduce carbon footprint in the iron and steel industry. *Johnson Matthey Technol. Rev.* **2018**, *62*, 395 - 402.
14. Cavani, F.; Trifirò, F.; Vaccari, A. Hydrotalcite-type anionic clays: Preparation, properties and applications. *Catal. Today* **1991**, *11*, 173 - 301.
15. Li, C.; Wei, M.; Evans, D. G.; Duan, X. Layered double hydroxide-based nanomaterials as highly efficient catalysts and adsorbents. *Small* **2014**, *10*, 4469 - 4486.

16. Panda, H. S.; Srivastava, R.; Bahadur, D. In-vitro release kinetics and stability of anticardiovascular drugs-intercalated layered double hydroxide nanohybrids. *J. Phys. Chem. B* **2009**, *113*, 15090 - 15100.
17. Theiss, F. L.; Ayoko, G. A.; Frost, R. L. Iodide removal using LDH technology. *Chem. Eng. J.* **2016**, *296*, 300 - 309.
18. Ram Reddy, M. K.; Xu, Z. P.; Lu, G. Q.; Diniz Da Costa, J. C. Influence of water on high-temperature CO<sub>2</sub> capture using layered double hydroxide derivatives. *Ind. Eng. Chem. Res.* **2008**, *47*, 2630 - 2635.
19. Ramírez-Moreno, M. J.; Romero-Ibarra, I. C.; Hernández-Pérez, M. A.; Pfeiffer, H. CO<sub>2</sub> adsorption at elevated pressure and temperature on Mg-Al layered double hydroxide. *Ind. Eng. Chem. Res.* **2014**, *53*, 8087 - 8094.
20. Wang, Q.; Tay, H. H.; Zhong, Z.; Luo, J.; Borgna, A. Synthesis of high-temperature CO<sub>2</sub> adsorbents from organo-layered double hydroxides with markedly improved CO<sub>2</sub> capture capacity. *Energy Environ. Sci.* **2012**, *5*, 7526 - 7530.
21. Wang, J.; Zhang, Y.; Altaf, N.; O'Hare, D.; Wang, Q. CHAPTER 1. Layered Double Hydroxides-derived Intermediate-temperature CO<sub>2</sub> Adsorbents. In *Pre-combustion Carbon Dioxide Capture Materials*; Inorganic Materials Series, Wang, Q.; The Royal Society of Chemistry, 2018; pp 1 - 60. doi:10.1039/9781788013390-00001.
22. Van Dijk, E.; Walspurger, S.; Cobden, P.; Van Den Brink, R. Testing of hydrotalcite based sorbents for CO<sub>2</sub> and H<sub>2</sub>S capture for use in sorption enhanced water gas shift. *Energy Procedia* **2011**, *4*, 1110 - 1117.

23. Singh, R.; Ram Reddy, M.K.; Wilson, S.; Joshi, K.; Diniz da Costa, J. C.; Webley, P. High temperature materials for CO<sub>2</sub> capture. *Energy Procedia* **2009**, *1*, 623 - 630.
24. Manohara, G. V.; Maroto-Valer, M. M.; Garcia, S. The effect of the layer-interlayer chemistry of LDHs on developing high temperature carbon capture materials. *Dalton Trans.* **2020**, *49*, 923 - 931.
25. Manohara, G. V. Exfoliation of layered double hydroxides (LDHs): A new route to mineralize atmospheric CO<sub>2</sub>. *RSC Adv.* **2014**, *4*, 46126 - 46132.
26. Wong, Y. T. A.; Martins, V.; Lucier, B. E. G.; Huang, Y. Solid-State NMR Spectroscopy: A Powerful Technique to Directly Study Small Gas Molecules Adsorbed in Metal–Organic Frameworks. *Chem. Eur. J.* **2019**, *25*, 1848 - 1853.
27. Lucier, B. E. G.; Chan, H.; Zhang, Y.; Huang, Y. Multiple Modes of Motion: Realizing the Dynamics of CO Adsorbed in M-MOF-74 (M = Mg, Zn) by Using Solid-State NMR Spectroscopy. *Eur. J. Inorg. Chem.* **2016**, 2017 - 2024.
28. Werner, M.; Rothermel, N.; Breitzke, H.; Gutmann, T.; Buntkowsky, G. Recent Advances in Solid State NMR of Small Molecules in Confinement. *Isr. J. Chem.* **2014**, *54*, 60 - 73.
29. Milner, P. J.; Siegelman, R. L.; Forse, A. C.; Gonzalez, M. I.; Runčevski, T.; Martell, J. D.; Reimer, J. A.; Long, J. R. A Diaminopropane-Appended Metal-Organic Framework Enabling Efficient CO<sub>2</sub> Capture from Coal Flue Gas via a Mixed Adsorption Mechanism. *J. Am. Chem. Soc.* **2017**, *139*, 13541 - 13553.
30. Forse, A. C.; Milner, P. J.; Lee, J.; Redfearn, H. N.; Oktawiec, J.; Siegelman, R. L.; Martell, J. D.; Dinakar, B.; Zasada, L. B.; Gonzalez, M. I.; Neaton, J. B.; Long, J. R.; Reimer, J. A.

Elucidating CO<sub>2</sub> Chemisorption in Diamine-Appended Metal–Organic Frameworks. *J. Am. Chem. Soc.* **2018**, *140*, 18016 - 18031.

31. Marti, R. M.; Howe, J. D.; Morelock, C. R.; Conradi, M. S.; Walton, K. S.; Sholl, D. S.; Hayes, S. E. CO<sub>2</sub> dynamics in pure and mixed-metal MOFs with open metal sites. *J. Phys. Chem. C* **2017**, *121*, 25778 - 25787.

32. Wittmann, T.; Tschense, C. B. L.; Zappe, L.; Koschnick, C.; Siegel, R.; Stäglich, R.; Lotsch, B. V.; Senker, J. Selective host-guest interactions in metal-organic frameworks: Via multiple hydrogen bond donor-acceptor recognition sites. *J. Mater. Chem. A* **2019**, *7*, 10379 - 10388.

33. Nielsen, U. G. Solid state NMR studies of photoluminescent. *Annu. Rep. NMR Spectrosc.* **2021**, *104*, 75 - 140.

34. Massiot, D.; Fayon, F.; Capron, M.; King, I.J.; Le Calvé, S.; Alonso, B.; Durand, J.; Bujoli, B.; Gan, Z.; Hoatson, G.L. Modelling one- and two-dimensional solid-state NMR spectra. *Magn. Reson. Chem.* **2002**, *40*, 70 - 76.

35. Cory, D. G.; Ritchey, W. M. Suppression of signals from the probe in bloch decay spectra. *J. Magn. Reson.* **1988**, *80*, 128 - 132.

36. Bielecki, A.; Kolbert, A. C.; Levitt, M. H. Frequency-switched pulse sequences: Homonuclear decoupling and dilute spin NMR in solids. *Chem. Phys. Lett.* **1989**, *155*, 341 - 346.

37. Amoureux, J. P.; Fernandez, C.; Steuernagel, S. Z Filtering in MQMAS NMR. *J. Magn. Reson., Ser. A* **1996**, *123*, 116 - 118.

38. Wobbe, M. C. C.; Kerridge, A.; Zwijnenburg, M. A. Optical excitation of MgO nanoparticles; a computational perspective. *Phys. Chem. Chem. Phys.* **2014**, *16*, 22052 - 22061.
39. Bawaa, F.; Panasb, I. Limiting properties of  $(\text{MgO})_n$  and  $(\text{CaO})_n$  clusters. *Phys. Chem. Chem. Phys.*, **2001**, *3*, 3042 - 3047.
40. Rassolov, V. A.; Ratner, M. A.; Pople, J. A.; Redfern, P. C.; Curtiss, L. A. 6-31G\* basis set for third-row atoms. *J. Comput. Chem.* **2001**, *22*, 976 - 984.
41. Huber, S. P.; Zoupanos, S.; Uhrin, M.; Talirz, L.; Kahle, L.; Häuselmann, R.; Gresch, D.; Müller, T.; Yakutovich, A. V.; Andersen, C. W.; Ramirez, F. F.; Adorf, C. S.; Gargiulo, F.; Kumbhar, S.; Passaro, E.; Johnston, C.; Merkys, A.; Cepellotti, A.; Mounet, N.; Marzari, N.; Kozinsky, B.; Pizzi, G. AiiDA 1.0, a scalable computational infrastructure for automated reproducible workflows and data provenance. *Sci. Data* **2020**, *7*, 300.
42. Frisch, M. J.; Trucks, G. W.; Schlegel, H. B.; Scuseria, G. E.; Robb, M. A.; Cheeseman, J. R.; Scalmani, G.; Barone, V.; Petersson, G. A.; Nakatsuji, H.; Li, X.; Caricato, M.; Marenich, A. V.; Bloino, J.; Janesko, B. G.; Gomperts, R.; Mennucci, B.; Hratchian, H. P.; Ortiz, J. V.; Izmaylov, A. F.; Sonnenberg, J. L.; Williams-Young, D.; Ding, F.; Lipparini, F.; Egidi, F.; Goings, J.; Peng, B.; Petrone, A.; Henderson, T.; Ranasinghe, D.; Zakrzewski, V. G.; Gao, J.; Rega, N.; Zheng, G.; Liang, W.; Hada, M.; Ehara, M.; Toyota, K.; Fukuda, R.; Hasegawa, J.; Ishida, M.; Nakajima, T.; Honda, Y.; Kitao, O.; Nakai, H.; Vreven, T.; Throssell, K.; Montgomery, J. A., Jr.; Peralta, J. E.; Ogliaro, F.; Bearpark, M. J.; Heyd, J. J.; Brothers, E. N.; Kudin, K. N.; Staroverov, V. N.; Keith, T. A.; Kobayashi, R.; Normand, J.; Raghavachari, K.; Rendell, A. P.; Burant, J. C.; Iyengar, S. S.; Tomasi, J.; Cossi, M.; Millam, J. M.; Klene, M.; Adamo, C.; Cammi, R.; Ochterski,

J. W.; Martin, R. L.; Morokuma, K.; Farkas, O.; Foresman, J. B.; Fox, D. J. *Gaussian 16*, Revision C.01; Gaussian, Inc.: Wallingford CT, **2016**.

43. Wolinski, K.; Hinton, J. F.; Pulay, P. Efficient Implementation of the Gauge-Independent Atomic Orbital Method for NMR Chemical Shift Calculations. *J. Am. Chem. Soc.* **1990**, *112*, 8251 - 8260.

44. Sahoo, P.; Ishihara, S.; Yamada, K.; Deguchi, K.; Ohki, S.; Tansho, M.; Shimizu, T.; Eisaku, N.; Sasai, R.; Labuta, J.; Ishikawa, D.; Hill, J. P.; Ariga, K.; Bastakoti, B. P.; Yamauchi, Y.; Iyi, N. Rapid Exchange between Atmospheric CO<sub>2</sub> and Carbonate Anion Intercalated within Magnesium Rich Layered Double Hydroxide. *ACS Appl. Mater. Interfaces* **2014**, *6*, 18352 - 18359.

45. Fu, Y.; Zhang, L.; Yue, B.; Chen, X.; He, H. Simultaneous Characterization of Solid Acidity and Basicity of Metal Oxide Catalysts via the Solid-State NMR Technique. *J. Phys. Chem. C* **2018**, *122*, 24094 - 24102.

46. Moore, J. K.; Surface, J. A.; Brenner, A.; Skemer, P.; Conradi, M. S.; Hayes, S. E. Quantitative Identification of Metastable Magnesium Carbonate Minerals by Solid-State <sup>13</sup>C NMR Spectroscopy. *Environ. Sci. Technol.* **2015**, *49*, 657 - 664.

47. Cui, J.; Olmsted, D. L.; Mehta, A. K.; Asta, M.; Hayes, S. E. NMR Crystallography: Evaluation of Hydrogen Positions in Hydromagnesite by <sup>13</sup>C{<sup>1</sup>H} REDOR Solid-State NMR and Density Functional Theory Calculation of Chemical Shielding Tensors. *Angew. Chem. Int. Ed.* **2019**, *58*, 4210.

48. Gao, W.; Zhou, T.; Wang, Q. Controlled synthesis of MgO with diverse basic sites and its CO<sub>2</sub> capture mechanism under different adsorption conditions. *Chem. Eng. J.* **2018**, *336*, 710 - 720.
49. Sideris, P. J.; Blanc, F.; Gan, Z.; Grey, C. P. Identification of Cation Clustering in Mg–Al Layered Double Hydroxides Using Multinuclear Solid State Nuclear Magnetic Resonance Spectroscopy. *Chem. Mater.* **2012**, *24*, 2449 - 2461.
50. Sideris, P. J.; Nielsen, U. G.; Gan, Z.; Grey, C. P. Mg/Al Ordering in Layered Double Hydroxides Revealed by Multinuclear NMR Spectroscopy. **2008**, *321*, 113 - 117.
51. Mi, J.; Chen, X.; Zhang, Q.; Zheng, Y.; Xiao, Y.; Liu, F.; Aua, C.; Jiang, L. Mechanochemically synthesized MgAl layered double hydroxide nanosheets for efficient catalytic removal of carbonyl sulfide and H<sub>2</sub>S. *Chem. Commun.* **2019**, *55*, 9375 - 9378.
52. Rugg, G.; Genest, A.; Rö, N. DFT Variants for Mixed-Metal Oxides. Benchmarks Using Multi-Center Cluster Models. *J. Phys. Chem. A* **2018**, *122*, 7042 - 7050.
53. Grey, C. P.; Vega, A. J. Determination of the Quadrupole Coupling Constant of the Invisible Aluminum Spins in Zeolite HY with <sup>1</sup>H/<sup>27</sup>Al TRAPDOR NMR. *J. Am. Chem. Soc.* **1995**, *117*, 8232 - 8242.
54. Sahoo, P.; Ishihara, S.; Yamada, K.; Deguchi, K.; Ohki, S.; Tansho, M.; Shimizu, T.; Eisaku, N.; Sasai, R.; Labuta, J.; Ishikawa, D.; Hill, J. P.; Ariga, K.; Bastakoti, B. P.; Yamauchi, Y.; Iyi, N. Rapid Exchange between Atmospheric CO<sub>2</sub> and Carbonate Anion Intercalated within Magnesium Rich Layered Double Hydroxide. *ACS Appl. Mater. Interfaces* **2014**, *6*, 18352 - 18359.



55. Radha, S.; Navrotsky, A. Energetics of CO<sub>2</sub> Adsorption on Mg–Al Layered Double Hydroxides and Related Mixed Metal Oxides. *J. Phys. Chem. C* **2014**, *118*, 29836 - 29844.
56. Nityashree, N.; Manohara, G. V.; Maroto-Valer, M. M.; Garcia, S. Advanced High-Temperature CO<sub>2</sub> Sorbents with Improved Long-Term Cycling Stability. *ACS Appl. Mater. Interfaces* **2020**, *12*, 33765 - 33774.
57. Vyalikh, A.; Massiot, D.; Scheler, U. Structural characterisation of aluminium layered double hydroxides by <sup>27</sup>Al solid-state NMR. *Solid State Nucl. Magn. Reson.* **2009**, *36*, 19 - 23.
58. d'Espinose de Lacaillerie, J.-B.; Fretigny, C.; Massiot, D. MAS NMR spectra of quadrupolar nuclei in disordered solids: the Czjzek model. *J. Magn. Reson.* **2008**, *192*, 244 - 251.